Research Paper

Genome-wide association study identifies genetic factors that modify age at onset in Machado-Joseph disease

Fulya Akçimen[1,2], Sandra Martins[3,4], Calwing Liao[1,2], Cynthia V. Bourassa[2,5], Hélène Catoire[2,5], Garth A. Nicholson[6], Olaf Riess[7], Mafalda Raposo[8], Marcondes C. França[9], João Vasconcelos[10], Manuela Lima[8], Iscia Lopes-Cendes[11,12], Maria Luiza Saraiva-Pereira[13,14], Laura B. Jardim[13,15], Jorge Sequeiros[4,16,17], Patrick A. Dion[2,5], Guy A. Rouleau[1,2,5]

[1]Department of Human Genetics, McGill University, Montréal, Québec, Canada
[2]Montreal Neurological Institute and Hospital, McGill University, Montréal, Québec, Canada
[3]i3S – Instituto de Investigação e Inovação em Saúde, Universidade do Porto, Porto, Portugal
[4]IPATIMUP – Institute of Molecular Pathology and Immunology of the University of Porto, Porto, Portugal
[5]Department of Neurology and Neurosurgery, McGill University, Montréal, Québec, Canada
[6]University of Sydney, Department of Medicine, Concord Hospital, Concord, Australia
[7]Institute of Medical Genetics and Applied Genomics, University of Tuebingen, Tuebingen, Germany
[8]Faculdade de Ciências e Tecnologia, Universidade dos Açores e Instituto de Biologia Molecular e Celular (IBMC), Instituto de Investigação e Inovação em Saúde (i3S), Universidade do Porto, Porto, Portugal
[9]Department of Neurology, Faculty of Medical Sciences, UNICAMP, São Paulo, Campinas, Brazil
[10]School of Medical Sciences, Department of Medical Genetics and Genomic Medicine, University of Campinas (UNICAMP), São Paulo, Campinas, Brazil
[11]The Brazilian Institute of Neuroscience and Neurotechnology (BRAINN), São Paulo, Campinas, Brazil
[12]Departamento de Neurologia, Hospital do Divino Espírito Santo, Ponta Delgada, Portugal
[13]Medical Genetics Service, Hospital de Clínicas de Porto Alegre (HCPA), Porto Alegre, Brazil
[14] Departamento de Bioquímica – ICBS, Universidade Federal do Rio Grande do Sul (UFRGS), Porto Alegre, Brazil
[15] Departamento de Medicina Interna, Universidade Federal do Rio Grande do Sul (UFRGS), Porto Alegre, Brazil
[16]Institute for Molecular and Cell Biology (IBMC), Universidade do Porto, Porto, Portugal
[17]Instituto de Ciências Biomédicas Abel Salazar (ICBAS), Universidade do Porto, Porto, Portugal

Correspondence to: Guy A. Rouleau; **email:** guy.rouleau@mcgill.ca
Keywords: Machado-Joseph disease, GWAS, age at onset, *ATXN3*, modifier
Received: November 20, 2019 **Accepted:** January 27, 2020 **Published:** March 23, 2020

ABSTRACT

Machado-Joseph disease (MJD/SCA3) is the most common form of dominantly inherited ataxia worldwide. The disorder is caused by an expanded CAG repeat in the *ATXN3* gene. Past studies have revealed that the length of the expansion partly explains the disease age at onset (AO) variability of MJD, which is confirmed in this study (Pearson's correlation coefficient R^2 = 0.62). Using a total of 786 MJD patients from five different geographical origins, a genome-wide association study (GWAS) was conducted to identify additional AO modifying factors that could explain some of the residual AO variability. We identified nine suggestively associated loci ($P < 1 \times 10^{-5}$). These loci were enriched for genes involved in vesicle transport, olfactory signaling, and synaptic pathways. Furthermore, associations between AO and the *TRIM29* and *RAG* genes suggests that DNA repair mechanisms might be implicated in MJD pathogenesis. Our study demonstrates the existence of several additional genetic factors, along with CAG expansion, that may lead to a better understanding of the genotype-phenotype correlation in MJD.

INTRODUCTION

Machado-Joseph disease, also known as spinocerebellar ataxia type 3 (MJD/SCA3), is an autosomal dominant neurodegenerative disorder that is characterized by progressive cerebellar ataxia and pyramidal signs, which can be associated with a complex clinical picture and includes extrapyramidal signs or amyotrophy [1, 2]. MJD is caused by an abnormal CAG trinucleotide repeat expansion in exon 10 of the ataxin-3 gene (*ATXN3*), located at 14q32.1. Deleterious expansions (CAG_{exp}) consensually contain 61 to 87 CAG repeats, whereas wild type alleles (CAG_{nor}) range from 12 to 44 [2].

As with other diseases caused by repeat expansions, such as Huntington's disease (HD) and other spino-cerebellar ataxias, there is an inverse correlation between expanded repeat size and the age at which pathogenesis leads to disease onset [3]. Depending on the cohort structure, the size of the repeat expansion explains 55 to 70% of the age at onset (AO) variability in MJD, suggesting the existence of additional modifying factors [3, 4]. Although several genetic factors have been proposed as modifiers, such as CAG repeat size of normal *ATXN3* (SCA3), *HTT* (HD), *ATXN2* (SCA2) and *ATN1* (DRPLA) alleles, *APOE* status, and expression level of *HSP40* [4–6], these were not replicated by subsequent studies [7, 8]. Since CAG tract profile and allelic frequencies of the potential modifier loci can have unique characteristics in different populations, large collaborative studies are required to identify genetic modifiers in MJD, as well as replicate the findings of such studies [8].

Previously, Genetic Modifiers of Huntington's Disease (GeM-HD) Consortium carried out a GWA approach of HD individuals to reveal genetic modifiers of AO in HD [9, 10]. A total of eleven [9] and fourteen loci [10] were found to be associated with residual age at HD onset. In the present study, we performed the first GWAS to identify some possible genetic modifiers of AO in MJD. First, we assessed the relationship between AO and size of the expanded (CAG_{exp}) and normal (CAG_{nor}) alleles, biological sex and geographical origin. Next, we determined a residual AO for each subject, which is the difference between the measured AO and the predicted/estimated AO from expanded CAG repeat size alone. Using the residuals as a quantitative phenotype for a GWAS, we looked for genetic factors that modulate AO in MJD.

RESULTS

The inverse correlation between CAG_{exp} and age at onset

In the first phase of the study, the expanded *ATXN3*-CAG repeat lengths of 786 MJD patients were assessed. The mean (SD) CAG_{exp} size were Australia: 68.2 (±3.3), Brazil: 74.3 (3.9), Germany: 72.9 (±3.6), North America: 73 (±4.3) and Portugal: 72 (±4.0). Next, the relationship between AO and CAG_{exp} size, CAG_{nor} size, sex and ethnicity was examined (Supplementary Table 1). The previously observed negative correlation between *ATXN3* CAG_{exp} size and AO [3] was confirmed (Pearson's correlation coefficient $R^2 = 0.62$) (Figure 1). The CAG_{nor} size ($P = 0.39$), sex ($P = 0.02$) and geographic origin (P [Brazil] = 0.38, P [Germany] = 0.38, P [North America] = 0.33, P [Portugal] = 0.29) were not significant and their addition had little contribution to the model ($\Delta R^2 = 0.0072$). Residual AO for each sample was calculated and used as a quantitative phenotype to identify the modifiers of AO. The distribution of residual AO was close a theoretical normal distribution (Figure 1).

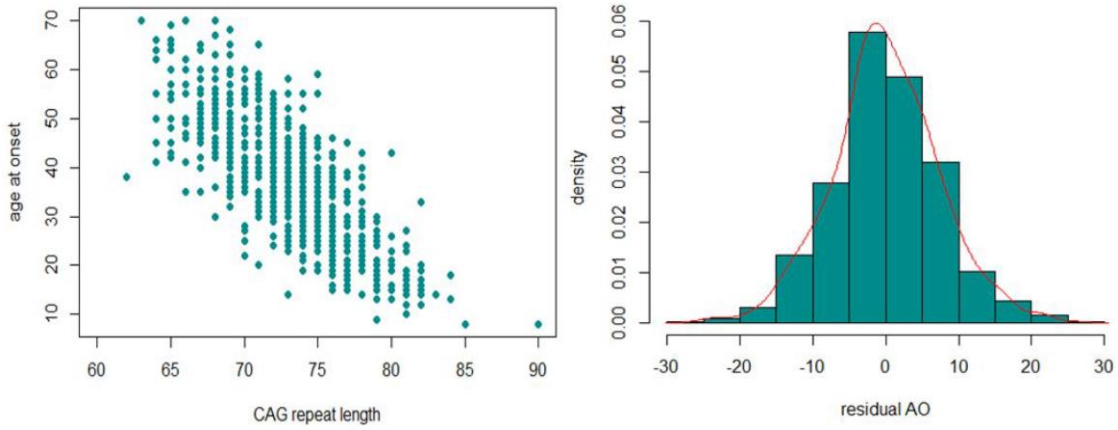

Figure 1. The inverse correlation between CAG_{exp} and AO (left) and the distribution of residual AO (right) observed in our MJD cohort.

Genome-wide association study

After post-imputation quality assessments, a total of 700 individuals with genotyping information for 6,716,580 variants remained for GWAS. The Manhattan plots are shown in Figure 2. The genomic inflation factor was close to one ($\lambda = 0.98$), indicating the p-values were not inflated. Genome-wide suggestive associations ($P < 1 \times 10^{-5}$) with 204 variants across 9 loci were identified (Supplementary Table 3). The most significantly associated SNP at each locus are shown in Table 1. Positional gene mapping aligned SNPs to 17 genes by their genomic location. Fourteen of the 204 variants had a Combined Annotation Dependent Depletion (CADD)-PHRED score higher than the suggested threshold for deleterious SNPs (12.37), arguing the given loci have a functional role [11].

Interaction analysis between CAG_{exp}, sex and SNP genotype

To assess a possible interaction between CAG_{exp} size and the variants identified, each of the nine variants was added to the initial linear regression, modelling AO as a function of CAG_{exp} size, SNP, sex, the first three principal components, CAG_{nor} size, interactions of SNP:CAG_{exp} and SNP:sex. Association of each independent SNP with AO revealed nominally significant p-values (P [rs7480166] = 8.42×10^{-6}, P [rs62171220] = 6.33×10^{-3}, P [rs2067390] = 4.51×10^{-5}, P [rs144891322] = 1.14×10^{-5}, P [rs11529293] = 1.62×10^{-5}, P [rs585809] = 2.91×10^{-5}, P [rs72660056] = 1.66×10^{-3}, P [rs11857349] = 8.21×10^{-6}, P [rs8141510] = 1.33×10^{-3}). With the addition of the identified variants to the model, correlation coefficient R^2 increased to 0.71 ($\Delta R^2 = 0.082$). Among the nine variants, only rs585809 (mapped to *TRIM29*) had a significant interaction with CAG_{exp} (P = 0.01), suggesting that rs585809 might modulate AO through this epistatic interaction on CAG_{exp}. The addition of SNP:sex interaction had little contribution to the model ($\Delta R^2 = 0.005$).

Association of HD-AO modifier variants in MJD

Association of previously identified HD-AO modifier loci in MJD were assessed. Among the 25 HD-AO modifier variants in 17 loci, a total of 18 variants (MAF > 0.02) in 12 loci were tested in this study (Supplementary Table 4). None of these HD-AO modifiers reached the genome-wide suggestive threshold. However, two variants rs144287831 (P = 0.02, effect size = - 0.98) and rs1799977 (P = 0.02, effect size = - 0.98) in the *MLH1* locus were found to be nominally associated with a later AO in MJD.

Pathway and gene-set enrichment analysis

A gene-set enrichment and pathway analysis was conducted using i-GSEA4GWAS v2 [12]. Various approaches and algorithms are currently in use to conduct similar analyses. To be able to make better comparisons with other studies that may use different approaches, we performed a secondary gene-set enrichment and pathway analysis using the VEGAS2 [13] and PASCAL [14] software (Supplementary Tables 5–7). We also used these results for replication

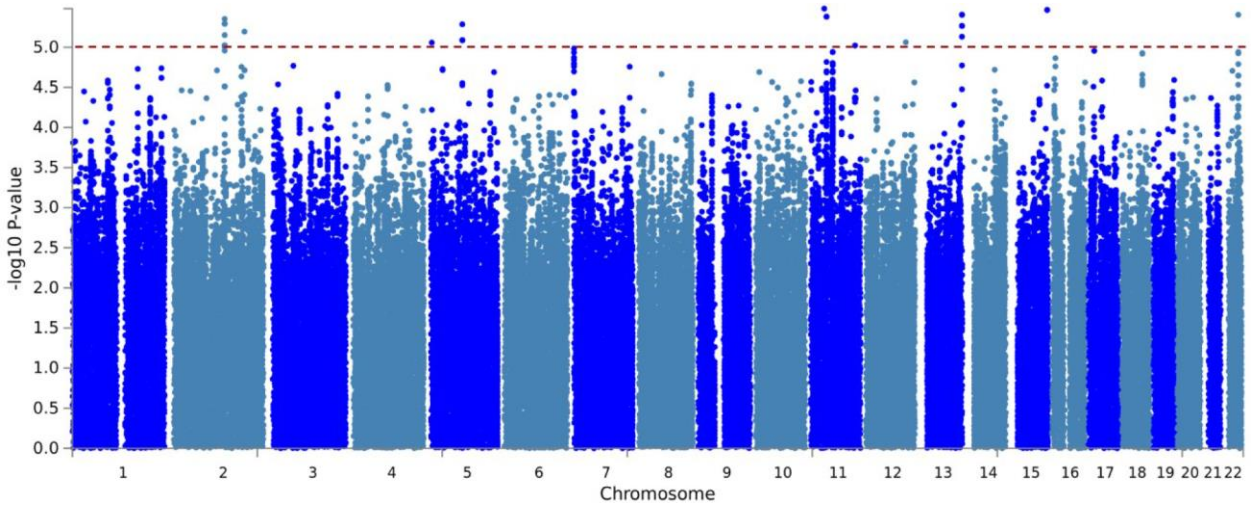

Figure 2. Manhattan plot of the GWAS for residual AO of MJD. Imputed using the HRC panel, 6,716,580 variants that passed QC are included in the plot. The x-axis shows the physical position along the genome. The y-axis shows the $-\log_{10}$(p-value) for association. The red line indicates the level of genome-wide suggestive association ($P = 1 \times 10^{-5}$).

Table 1. Suggestive loci associated with residual age at onset in MJD. Chr: chromosome, MAF: minor allele frequency, 1KGP: 1000 Genomes Project.

SNP	Chr	Position (GRCh37)	Nearest gene	Minor allele	Major allele	MJD MAF	1KGP MAF	b (SNP effect)	P-value
rs62171220	2	137802855	*THSD7B*	G	C	0.13	0.11	2.71	4.45×10^{-6}
rs2067390	2	191209028	*HIBCH, INPP1*	A	T	0.04	0.06	4.74	6.39×10^{-6}
rs144891322	5	85135387	*RPL5P17,*	C	T	0.02	0.007	6.10	5.18×10^{-6}
rs11529293	11	36855388	*C11orf74, RAG1, RAG2*	T	C	0.14	0.26	-2.71	3.30×10^{-6}
rs7480166	11	42984753	*HNRNPKP3*	A	G	0.40	0.40	-1.86	4.17×10^{-6}
rs585809	11	119949979	*TRIM29*	T	C	0.06	0.17	-3.76	9.50×10^{-6}
rs72660056	13	113507543	*ATP11A*	A	G	0.08	0.05	-3.29	3.94×10^{-6}
rs11857349	15	99924857	*TTC23, SYNM, LRRC28*	G	A	0.04	0.02	-4.58	3.43×10^{-6}
rs8141510	22	42821185	*NFAM1, CYP2D6, NAGA, NDUFA6*	C	T	0.43	0.49	1.83	3.94×10^{-6}

Table 2. Pathways significant after multiple-correction ($q < 5 \times 10^{-2}$) in the primary GSEA analysis and replicated using at least one of the secondary gene-set enrichment algorithms. NA means that the pathway was not enriched by at least two significant genes in VEGAS.

Pathway	Description	p-value (GSEA)	q-value (GSEA)	p-value (VEGAS)	permuted p-value (VEGAS)	p-value (PASCAL)
GO:0030133	transport vesicle	$< 1.0 \times 10^{-3}$	8.20×10^{-3}	6.15×10^{-40}	4.46×10^{-1}	6.70×10^{-3}
KEGG:04740	olfactory transduction	$< 1.0 \times 10^{-3}$	8.30×10^{-3}	NA	NA	3.89×10^{-4}
R-HSA:381753	olfactory signaling pathway	$< 1.0 \times 10^{-3}$	8.80×10^{-3}	1.10×10^{-27}	7.71×10^{-1}	2.51×10^{-4}
GO:0044456	synapse part	$< 1.0 \times 10^{-3}$	9.30×10^{-3}	1.25×10^{-182}	$< 1.0 \times 10^{-6}$	$< 1.0 \times 10^{-7}$
R-HSA:74217	purine salvage	$< 1.0 \times 10^{-3}$	1.06×10^{-2}	1.06×10^{-2}	2.15×10^{-1}	6.48×10^{-3}
GO:0045202	synapse	$< 1.0 \times 10^{-3}$	1.15×10^{-2}	1.15×10^{-2}	$< 1.0 \times 10^{-6}$	$< 1.0 \times 10^{-7}$
GO:0004177	aminopeptidase activity	$< 1.0 \times 10^{-3}$	1.50×10^{-2}	1.50×10^{-2}	3.41×10^{-1}	1.24×10^{-2}
GO:0008238	exopeptidase activity	$< 1.0 \times 10^{-3}$	1.80×10^{-2}	1.80×10^{-2}	2.80×10^{-2}	8.31×10^{-3}
GO:0006898	receptor mediated endocytosis	$< 1.0 \times 10^{-3}$	2.25×10^{-2}	2.25×10^{-2}	2.03×10^{-1}	6.64×10^{-3}
GO:0016917	GABA receptor activity	$< 1.0 \times 10^{-3}$	2.26×10^{-2}	2.26×10^{-2}	1.30×10^{-4}	2.30×10^{-5}
GO:0030140	trans Golgi network transport vesicle	$< 1.0 \times 10^{-3}$	2.36×10^{-2}	2.36×10^{-2}	2.80×10^{-2}	1.28×10^{-1}
GO:0009725	response to hormone stimulus	$< 1.0 \times 10^{-3}$	2.73×10^{-2}	2.73×10^{-2}	1.32×10^{-1}	1.30×10^{-4}
GO:0030425	Dendrite	$< 1.0 \times 10^{-3}$	3.86×10^{-2}	3.86×10^{-2}	$< 1.0 \times 10^{-6}$	$< 1.0 \times 10^{-7}$

purposes in our own study. A total of 13 overrepresented pathways were found, after FDR-multiple testing correction (q-value < 0.05) in the primary GSEA analysis and replicated using at least one of the secondary gene-set enrichment algorithms (Table 2). Overall, the most significantly enriched gene-sets and pathways were vesicle transport, olfactory signaling, and synaptic pathways. Visualization and clustering of pathways are shown in Figure 3.

DISCUSSION

Using five cohorts from different geographical origins, we performed the first GWAS to examine the presence of genetic factors that could modify AO in MJD. We identified a total of nine loci that were potentially associated with either an earlier or later AO. Concomitantly, we confirmed the previously observed negative correlation between CAG_{exp} and AO [3]. It was shown previously that normal *ATXN3* allele (CAG_{nor}) had a significant influence on AO of MJD [15]; however, several studies did not replicate this effect [6, 8]. Indeed, we did not observe an association between CAG_{nor} and AO. However, it had little contribution to our model, with a minor difference in the correlation coefficient ($\Delta R^2 = 0.0012$).

In our GWAS, the strongest signal is for the rs11529293 variant ($P = 3.30 \times 10^{-6}$) within the *C11orf72* and *RAG* loci at 11p12. Within this locus, two *RAG* genes, recombination-activating genes *RAG1* and *RAG2*, were shown to be implicated in DNA damage response and DNA repair machineries [16, 17]. The rs585809 variant, which was mapped to the *TRIM29* gene, was found to interact with CAG_{exp}, suggesting that it might have an effect on AO through this interaction. Both *RAG* and *TRIM29* loci were identified as AO-hastening modifiers. *TRIM29* encodes for tripartite motif protein 29, which is implicated in mismatch repair and double strand breaks pathways [18, 19]. TRIM29 is involved both upstream and downstream of these pathways, in the regulation of DNA repair proteins into chromatin by mediating the interaction between them. One of these DNA repair proteins is MLH1, which is implicated in mismatch repair complex [19]. Previously, the *MLH1* locus was identified as an AO modifier in another neurodegenerative disease caused by CAG repeat expansion, Huntington's disease [9, 10, 20]. Additionally, in a genome-wide genetic screening study, MLH1-knock out was shown to modify the somatic expansion of the CAG repeat and slow the pathogenic process in HD mouse model [21].

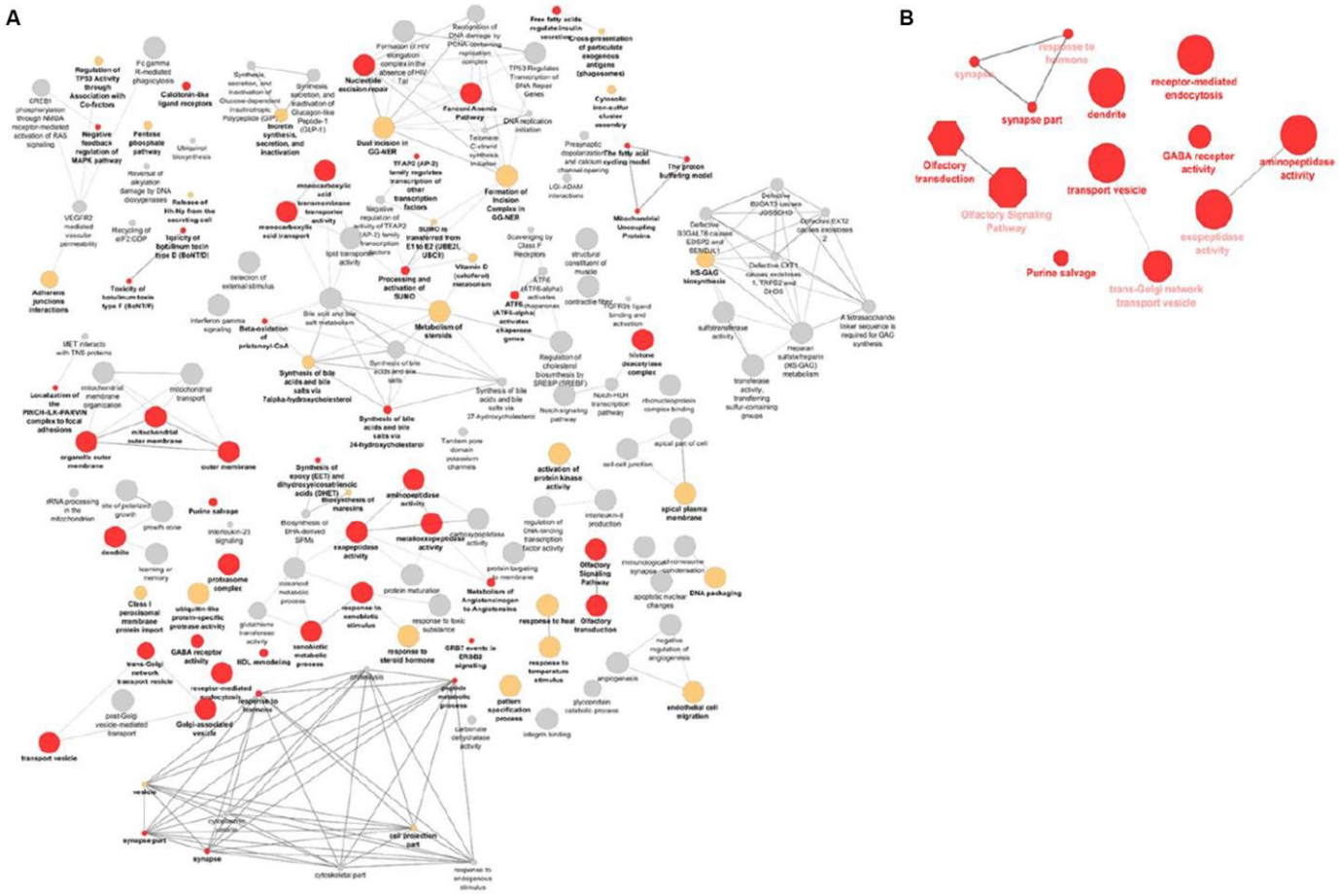

Figure 3. Visualization of the gene-sets and pathways enriched in primary GSEA analysis (**A**) and replicated in VEGAS and PASCAL (**B**). The size of the nodes corresponds to the number of the genes associated with a term. The significance is represented by the color of the nodes ($P < 0.05$, $0.05 < P < 0.1$ and $P > 0.1$ are represented by red, yellow and gray, respectively).

Overall, the association of *TRIM29* and *RAG* loci suggests that DNA repair mechanisms may be implicated in the alteration of AO of MJD, as well as HD, and may have a role in the pathogenesis of other CAG repeat diseases. Interestingly, in a previous study, we found variants in three transcription-coupled repair genes (ERCC6, RPA, and CDK7) associated with different CAG instability patterns in MJD [22].

We identified gene-sets enriched in olfactory signaling, vesicle transport, and synaptic pathways. Olfactory dysfunction is one of the main non-motor symptoms that was already described in patients with MJD [23, 24]. In a previous study, transplantation of olfactory ensheathing cells, which are specialized glial cells of the primary olfactory system, were found to improve motor function in an MJD mice model, and were suggested as a novel potential strategy for MJD treatment [25]. Vesicle transport and synaptic pathways were also implicated in MJD, as well as in other neurodegenerative diseases [26, 27]. An interruption of synaptic transmission caused by an expanded polyglutamine repeat and mutant ataxin-3 aggregates were shown in *Drosophila* and *Caenorhabditis elegans* models of MJD. Therefore, the interaction between synaptic vesicles and mutant aggregates supports the role of synaptic vesicle transport in the pathogenesis of MJD [28, 29]. Overall, we suggest that these gene-sets and pathways might construct a larger molecular network that could modulate the AO in MJD.

In summary, our study identified nine genetic loci that may modify the AO of MJD. Identification of *TRIM29* and *RAG* genetic variants, as well as our gene-set enrichment analyses, implicated DNA repair, olfactory signaling, synaptic, and vesicle transport pathways in the pathogenesis of MJD. Although we used different cohorts from five distinct geographical ethnicities, a replication study in similar or additional populations would add valuable evidence to support our findings.

MATERIALS AND METHODS

Study subjects

A total of 786 MJD patients from five distinct geographical origins (Portugal, Brazil, North America, Germany and Australia) were included in the present study. The overall average age at onset (standard deviation) was 38 (± 1.82) years, with a 1:1 male to female ratio. All subjects provided informed consent, and the study was approved by the respective institutional review boards. Detailed cohort demographics are shown in Supplementary Table 2.

Assessment of the *ATXN3* CAG repeat length

A singleplex polymerase chain reaction was performed to determine the length of the CAG_{exp} and CAG_{nor} alleles at exon 10 of *ATXN3* [30]. The final volume for each assay was 10 µL: 7.5 ng of gDNA, 0.2 µM of each primer, 5 µL of Taq PCR Master Mix Kit Qiagen®, 1 µL of Q-Solution from Qiagen® and H_2O. Fragment length analysis was done using ABIPrism 3730xl sequencer (Applied Biosystems®, McGill University and Genome Québec Innovation Centre) and GeneMapper software [31]. A stepwise regression model was performed to assess the correlation between AO and CAG_{exp} size, as well as gender, origin, CAG_{nor} size, and interaction between these variables. Residual AO was calculated for each subject by subtracting individual's expected AO based upon CAG_{exp} size from actual AO, to be used as the primary phenotype for following genetic approach.

Genotyping, quality control and imputation

Samples were genotyped using the Global Screening Array v.1.0 from Illumina (636,139 markers). Sample-based (missingness, relatedness, sex, and multi-dimensional scaling analysis) and SNP-based quality assessments (missingness, Hardy-Weinberg equilibrium, and minor allele frequency) were conducted using PLINK version 1.9 [32]. In sample level QC, samples were excluded with one or more of the following: high missingness (missingness rate > 0.05), close relationship (pi-hat value > 0.2), discrepancy between genetically-inferred sex and reported sex, population outliers (deviation ≥ 4 SD from the population mean in multidimensional scaling analysis). All SNPs were checked for marker genotyping call rate (> 98%), minor allele frequency (MAF) > 0.05, and HWE (p-value threshold = 1.0×10^{-5}).

Phasing and imputation were performed using SHAPEIT [33] and PBWT [34] pipelines, implemented on the Sanger Imputation Service [35]. Haplotype Reference Consortium (HRC) reference panel r1.1 containing 64,940 human haplotypes at 40,405,505 genetic markers were used as the reference panel. Imputed variants with an allele count of 30 (MAF > 0.02), an imputation quality score above 0.3 and an HWE p-value of > 1.0×10^{-5} were included for subsequent analysis.

Genome-wide association analysis

A genome-wide linear mixed model based association analysis was conducted using –mlma-loco option of GCTA version 1.91.7 [36]. Residual AO was modelled as a function of minor allele count of the test SNP, sex, and the first three principal components

based on the scree plot (Supplementary Figure 1). Manhattan plots were generated in FUMA v.1.3.4 [37]. Regional association plots were generated using LocusZoom [38] (Supplementary Figure 2).

Functional annotation of SNPs

Genomic risk loci were defined using SNP2GENE function implemented in FUMA. Independent suggestive SNPs ($P < 1 \times 10^{-5}$) with a threshold of $r^2 < 0.6$ were selected within a 250 kb window. The UK Biobank release 2 European population consisting of randomly selected 10,000 subjects was used as the reference population panel. The ANNOVAR [39] categories and combined annotation-dependent depletion (CADD) [40] scores were obtained from FUMA for functional annotation. Functionally annotated variants were mapped to genes based on genomic position using FUMA positional mapping tool.

Pathway analysis

To identify known biological pathways and gene sets at the associated loci, an enrichment approach was applied using public datasets containing Gene Ontology (GO, http://geneontology.org), the Kyoto Encyclopaedia of Genes and Genomes (KEGG, https://www.genome.jp/kegg) and Reactome (https://reactome.org) pathways. The primary enrichment analysis was performed using the i-GSEA4GWAS v2. It uses a candidate list of a genome-wide set of genes mapped within the SNP loci and ranks them based on the strength of their association with the phenotype. Genes were mapped within 20 kb up or downstream of the SNPs with a $P < 0.05$. Gene and pathway sets meeting a false discovery rate *(FDR)*-corrected q-value < 0.05 were regarded as significantly associated with high confidence, and q-value < 0.25 was regarded to be possibly associated with the phenotype of interest. We performed a secondary gene-based association test using the Versatile Gene-based Association Study (VEGAS) algorithm that controls the number of SNPs in each gene and the linkage disequilibrium (LD) between these SNPs using the HapMap European population. As a third algorithm to identify enriched pathways, we used Pathway Scoring Algorithm (PASCAL), which controls for potential bias from gene size, SNP density, as well as LD. ClueGO [41] and CluePedia [42] plug-ins in Cytoscape were employed to visualize identified pathways and their clustering.

ACKNOWLEDGMENTS

The authors thank the participants for their contribution to the study. The authors would like to thank Jay P. Ross, Faezeh Sarayloo, Zoe Schmilovich and S. Can Akerman for their assistance in reviewing the manuscript and scientific content.

CONFLICTS OF INTEREST

The authors declare no conflicts of interest.

FUNDING

FA and CL were funded by the Fonds de Recherche du Québec–Santé. SM is funded by FCT (CEECIND/00684/2017) and by NORTE-01-0145-FEDER-000008, supported by Norte Portugal Regional Programme (NORTE 2020), under the PORTUGAL 2020 Partnership Agreement, through the European Regional Development Fund (ERDF). FM and LI are funded by Fundaçao de Amparo a Pesquisa do Estado de São Paulo (FAPESP, 2013/07559-3). MLSP and LBJ were funded by Conselho Nacional de Desenvolvimento Científico e Tecnológico, Brazil (CNPq) and by Coordenação de Aperfeiçoamento de Pessoal de Nível Superior (CAPES). GAR holds a Canada Research Chair in Genetics of the Nervous System and the Wilder Penfield Chair in Neurosciences.

REFERENCES

1. Twist EC, Casaubon LK, Ruttledge MH, Rao VS, Macleod PM, Radvany J, Zhao Z, Rosenberg RN, Farrer LA, Rouleau GA. Machado Joseph disease maps to the same region of chromosome 14 as the spinocerebellar ataxia type 3 locus. J Med Genet. 1995; 32:25–31. https://doi.org/10.1136/jmg.32.1.25 PMID:7897622

2. Bettencourt C, Lima M. Machado-Joseph Disease: from first descriptions to new perspectives. Orphanet J Rare Dis. 2011; 6:35. https://doi.org/10.1186/1750-1172-6-35 PMID:21635785

3. Maciel P, Gaspar C, DeStefano AL, Silveira I, Coutinho P, Radvany J, Dawson DM, Sudarsky L, Guimarães J, Loureiro JE, et al. Correlation between CAG repeat length and clinical features in Machado-Joseph disease. Am J Hum Genet. 1995; 57:54–61. PMID:7611296

4. de Mattos EP, Kolbe Musskopf M, Bielefeldt Leotti V, Saraiva-Pereira ML, Jardim LB. Genetic risk factors for modulation of age at onset in Machado-Joseph disease/spinocerebellar ataxia type 3: a systematic review and meta-analysis. J Neurol Neurosurg Psychiatry. 2019; 90:203–10. https://doi.org/10.1136/jnnp-2018-319200 PMID:30337442

5. Zijlstra MP, Rujano MA, Van Waarde MA, Vis E, Brunt ER, Kampinga HH. Levels of DNAJB family members (HSP40) correlate with disease onset in patients with spinocerebellar ataxia type 3. Eur J Neurosci. 2010; 32:760–70. https://doi.org/10.1111/j.1460-9568.2010.07352.x PMID:20726892

6. Tezenas du Montcel S, Durr A, Bauer P, Figueroa KP, Ichikawa Y, Brussino A, Forlani S, Rakowicz M, Schöls L, Mariotti C, van de Warrenburg BP, Orsi L, Giunti P, et al, and Clinical Research Consortium for Spinocerebellar Ataxia (CRC-SCA), and EUROSCA network. Modulation of the age at onset in spinocerebellar ataxia by CAG tracts in various genes. Brain. 2014; 137:2444–55. https://doi.org/10.1093/brain/awu174 PMID:24972706

7. Chen Z, Zheng C, Long Z, Cao L, Li X, Shang H, Yin X, Zhang B, Liu J, Ding D, Peng Y, Wang C, Peng H, et al, and Chinese Clinical Research Cooperative Group for Spinocerebellar Ataxias (CCRCG-SCA). (CAG)n loci as genetic modifiers of age-at-onset in patients with Machado-Joseph disease from mainland China. Brain. 2016; 139:e41–41. https://doi.org/10.1093/brain/aww087 PMID:27085188

8. Raposo M, Ramos A, Bettencourt C, Lima M. Replicating studies of genetic modifiers in spinocerebellar ataxia type 3: can homogeneous cohorts aid? Brain. 2015; 138:e398–398. https://doi.org/10.1093/brain/awv206 PMID:26173860

9. Lee JM, Wheeler VC, Chao MJ, Vonsattel JP, Pinto RM, Lucente D, Abu-Elneel K, Ramos EM, Mysore JS, Gillis T, MacDonald ME, Gusella JF, Harold D, et al, and Genetic Modifiers of Huntington's Disease (GeM-HD) Consortium. Identification of Genetic Factors that Modify Clinical Onset of Huntington's Disease. Cell. 2015; 162:516–26. https://doi.org/10.1016/j.cell.2015.07.003 PMID:26232222

10. Lee JM, Correia K, Loupe J, Kim KH, Barker D, Hong EP, Chao MJ, Long JD, Lucente D, Vonsattel JP, Pinto RM, Abu Elneel K, Ramos EM, et al, and Genetic Modifiers of Huntington's Disease (GeM-HD) Consortium. Electronic address: gusella@helix.mgh.harvard.edu, and Genetic Modifiers of Huntington's Disease (GeM-HD) Consortium. CAG Repeat Not Polyglutamine Length Determines Timing of Huntington's Disease Onset. Cell. 2019; 178:887–900.e14. https://doi.org/10.1016/j.cell.2019.06.036 PMID:31398342

11. Amendola LM, Dorschner MO, Robertson PD, Salama JS, Hart R, Shirts BH, Murray ML, Tokita MJ, Gallego CJ, Kim DS, Bennett JT, Crosslin DR, Ranchalis J, et al. Actionable exomic incidental findings in 6503 participants: challenges of variant classification. Genome Res. 2015; 25:305–15. https://doi.org/10.1101/gr.183483.114 PMID:25637381

12. Zhang K, Cui S, Chang S, Zhang L, Wang J. i-GSEA4GWAS: a web server for identification of pathways/gene sets associated with traits by applying an improved gene set enrichment analysis to genome-wide association study. Nucleic Acids Res. 2010; 38:W90–5. https://doi.org/10.1093/nar/gkq324 PMID:20435672

13. Mishra A, Macgregor S. VEGAS2: Software for More Flexible Gene-Based Testing. Twin Res Hum Genet. 2015; 18:86–91. https://doi.org/10.1017/thg.2014.79 PMID:25518859

14. Lamparter D, Marbach D, Rueedi R, Kutalik Z, Bergmann S. Fast and Rigorous Computation of Gene and Pathway Scores from SNP-Based Summary Statistics. PLoS Comput Biol. 2016; 12:e1004714. https://doi.org/10.1371/journal.pcbi.1004714 PMID:26808494

15. França MC Jr, Emmel VE, D'Abreu A, Maurer-Morelli CV, Secolin R, Bonadia LC, da Silva MS, Nucci A, Jardim LB, Saraiva-Pereira ML, Marques W Jr, Paulson H, Lopes-Cendes I. Normal ATXN3 Allele but Not CHIP Polymorphisms Modulates Age at Onset in Machado-Joseph Disease. Front Neurol. 2012; 3:164. https://doi.org/10.3389/fneur.2012.00164 PMID:23181052

16. Lescale C, Deriano L. The RAG recombinase: beyond breaking. Mech Ageing Dev. 2017; 165:3–9. https://doi.org/10.1016/j.mad.2016.11.003 PMID:27863852

17. Bahjat M, Guikema JE. The Complex Interplay between DNA Injury and Repair in Enzymatically Induced Mutagenesis and DNA Damage in B Lymphocytes. Int J Mol Sci. 2017; 18:18. https://doi.org/10.3390/ijms18091876 PMID:28867784

18. Wikiniyadhanee R, Lerksuthirat T, Stitchantrakul W, Chitphuk S, Dejsuphong D. AB064. TRIM29: a novel gene involved in DNA repair mechanisms. Ann Transl Med. 2017; 5:AB064–064. https://doi.org/10.21037/atm.2017.s064

19. Masuda Y, Takahashi H, Sato S, Tomomori-Sato C, Saraf A, Washburn MP, Florens L, Conaway RC, Conaway JW, Hatakeyama S. TRIM29 regulates the

assembly of DNA repair proteins into damaged chromatin. Nat Commun. 2015; 6:7299. https://doi.org/10.1038/ncomms8299 PMID:26095369

20. Lee JM, Chao MJ, Harold D, Abu Elneel K, Gillis T, Holmans P, Jones L, Orth M, Myers RH, Kwak S, Wheeler VC, MacDonald ME, Gusella JF. A modifier of Huntington's disease onset at the MLH1 locus. Hum Mol Genet. 2017; 26:3859–67. https://doi.org/10.1093/hmg/ddx286 PMID:28934397

21. Pinto RM, Dragileva E, Kirby A, Lloret A, Lopez E, St Claire J, Panigrahi GB, Hou C, Holloway K, Gillis T, Guide JR, Cohen PE, Li GM, et al. Mismatch repair genes Mlh1 and Mlh3 modify CAG instability in Huntington's disease mice: genome-wide and candidate approaches. PLoS Genet. 2013; 9:e1003930. https://doi.org/10.1371/journal.pgen.1003930 PMID:24204323

22. Martins S, Pearson CE, Coutinho P, Provost S, Amorim A, Dubé MP, Sequeiros J, Rouleau GA. Modifiers of (CAG)(n) instability in Machado-Joseph disease (MJD/SCA3) transmissions: an association study with DNA replication, repair and recombination genes. Hum Genet. 2014; 133:1311–18. https://doi.org/10.1007/s00439-014-1467-8 PMID:25026993

23. Braga-Neto P, Felicio AC, Pedroso JL, Dutra LA, Bertolucci PH, Gabbai AA, Barsottini OG. Clinical correlates of olfactory dysfunction in spinocerebellar ataxia type 3. Parkinsonism Relat Disord. 2011; 17:353–56. https://doi.org/10.1016/j.parkreldis.2011.02.004 PMID:21367642

24. Pedroso JL, França MC Jr, Braga-Neto P, D'Abreu A, Saraiva-Pereira ML, Saute JA, Teive HA, Caramelli P, Jardim LB, Lopes-Cendes I, Barsottini OG. Nonmotor and extracerebellar features in Machado-Joseph disease: a review. Mov Disord. 2013; 28:1200–08. https://doi.org/10.1002/mds.25513 PMID:23775899

25. Hsieh J, Liu JW, Harn HJ, Hsueh KW, Rajamani K, Deng YC, Chia CM, Shyu WC, Lin SZ, Chiou TW. Human Olfactory Ensheathing Cell Transplantation Improves Motor Function in a Mouse Model of Type 3 Spinocerebellar Ataxia. Cell Transplant. 2017; 26:1611–21. https://doi.org/10.1177/0963689717732578 PMID:29251109

26. Wiatr K, Piasecki P, Marczak Ł, Wojciechowski P, Kurkowiak M, Płoski R, Rydzanicz M, Handschuh L, Jungverdorben J, Brüstle O, Figlerowicz M, Figiel M. Altered Levels of Proteins and Phosphoproteins, in the Absence of Early Causative Transcriptional Changes, Shape the Molecular Pathogenesis in the Brain of Young Presymptomatic Ki91 SCA3/MJD Mouse. Mol Neurobiol. 2019; 56:8168–202. https://doi.org/10.1007/s12035-019-01643-4 PMID:31201651

27. Gissen P, Maher ER. Cargos and genes: insights into vesicular transport from inherited human disease. J Med Genet. 2007; 44:545–55. https://doi.org/10.1136/jmg.2007.050294 PMID:17526798

28. Gunawardena S, Goldstein LS. Polyglutamine diseases and transport problems: deadly traffic jams on neuronal highways. Arch Neurol. 2005; 62:46–51. https://doi.org/10.1001/archneur.62.1.46 PMID:15642849

29. Khan LA, Bauer PO, Miyazaki H, Lindenberg KS, Landwehrmeyer BG, Nukina N. Expanded polyglutamines impair synaptic transmission and ubiquitin-proteasome system in Caenorhabditis elegans. J Neurochem. 2006; 98:576–87. https://doi.org/10.1111/j.1471-4159.2006.03895.x PMID:16805848

30. Martins S, Calafell F, Wong VC, Sequeiros J, Amorim A. A multistep mutation mechanism drives the evolution of the CAG repeat at MJD/SCA3 locus. Eur J Hum Genet. 2006; 14:932–40. https://doi.org/10.1038/sj.ejhg.5201643 PMID:16724006

31. Chatterji S, Pachter L. Reference based annotation with GeneMapper. Genome Biol. 2006; 7:R29–29. https://doi.org/10.1186/gb-2006-7-4-r29 PMID:16600017

32. Chang CC, Chow CC, Tellier LC, Vattikuti S, Purcell SM, Lee JJ. Second-generation PLINK: rising to the challenge of larger and richer datasets. Gigascience. 2015; 4:7. https://doi.org/10.1186/s13742-015-0047-8 PMID:25722852

33. Delaneau O, Marchini J, Zagury JF. A linear complexity phasing method for thousands of genomes. Nat Methods. 2011; 9:179–81. https://doi.org/10.1038/nmeth.1785 PMID:22138821

34. Durbin R. Efficient haplotype matching and storage using the positional Burrows-Wheeler transform (PBWT). Bioinformatics. 2014; 30:1266–72. https://doi.org/10.1093/bioinformatics/btu014 PMID:24413527

35. McCarthy S, Das S, Kretzschmar W, Delaneau O, Wood AR, Teumer A, Kang HM, Fuchsberger C, Danecek P, Sharp K, Luo Y, Sidore C, Kwong A, et al, and Haplotype Reference Consortium. A reference

panel of 64,976 haplotypes for genotype imputation. Nat Genet. 2016; 48:1279–83. https://doi.org/10.1038/ng.3643 PMID:27548312

36. Yang J, Lee SH, Goddard ME, Visscher PM. GCTA: a tool for genome-wide complex trait analysis. Am J Hum Genet. 2011; 88:76–82. https://doi.org/10.1016/j.ajhg.2010.11.011 PMID:21167468

37. Watanabe K, Taskesen E, van Bochoven A, Posthuma D. Functional mapping and annotation of genetic associations with FUMA. Nat Commun. 2017; 8:1826. https://doi.org/10.1038/s41467-017-01261-5 PMID:29184056

38. Pruim RJ, Welch RP, Sanna S, Teslovich TM, Chines PS, Gliedt TP, Boehnke M, Abecasis GR, Willer CJ. LocusZoom: regional visualization of genome-wide association scan results. Bioinformatics. 2010; 26:2336–37. https://doi.org/10.1093/bioinformatics/btq419 PMID:20634204

39. Wang K, Li M, Hakonarson H. ANNOVAR: functional annotation of genetic variants from high-throughput sequencing data. Nucleic Acids Res. 2010; 38:e164. https://doi.org/10.1093/nar/gkq603 PMID:20601685

40. Rentzsch P, Witten D, Cooper GM, Shendure J, Kircher M. CADD: predicting the deleteriousness of variants throughout the human genome. Nucleic Acids Res. 2019; 47:D886–94. https://doi.org/10.1093/nar/gky1016 PMID:30371827

41. Bindea G, Mlecnik B, Hackl H, Charoentong P, Tosolini M, Kirilovsky A, Fridman WH, Pagès F, Trajanoski Z, Galon J. ClueGO: a Cytoscape plug-in to decipher functionally grouped gene ontology and pathway annotation networks. Bioinformatics. 2009; 25:1091–93. https://doi.org/10.1093/bioinformatics/btp101 PMID:19237447

42. Bindea G, Galon J, Mlecnik B. CluePedia Cytoscape plugin: pathway insights using integrated experimental and in silico data. Bioinformatics. 2013; 29:661–63. https://doi.org/10.1093/bioinformatics/btt019 PMID:23325622

SUPPLEMENTARY MATERIALS

Supplementary Figures

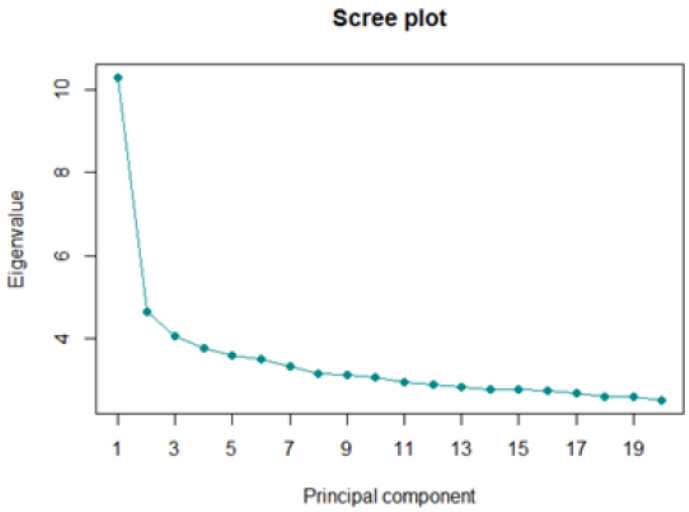

Supplementary Figure 1. Scree plot showing the eigenvalues of the first 20 principal components (PCs). This plot indicates that the first three PCs explain the majority of the variability in data.

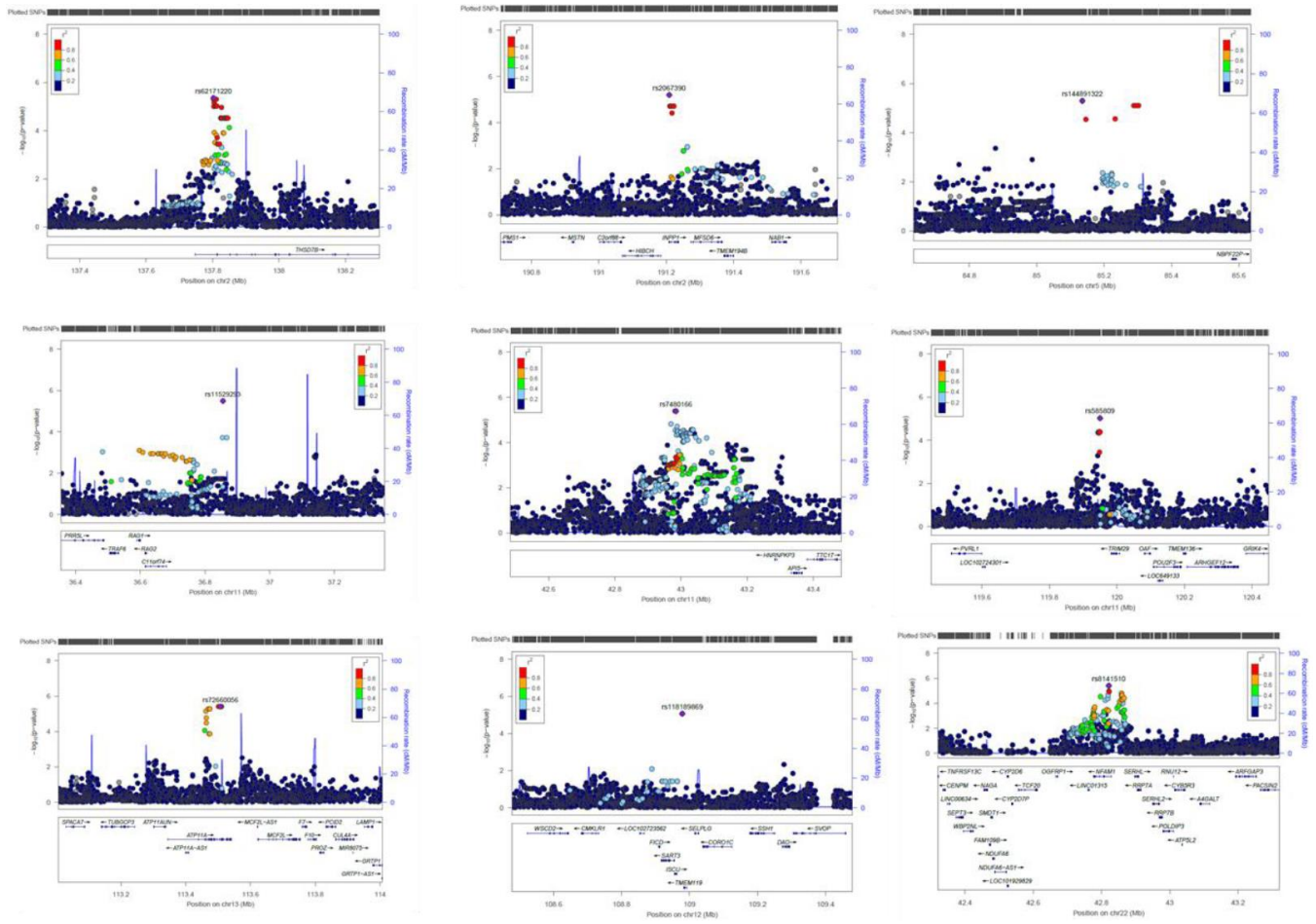

Supplementary Figure 2. Regional LocusZoom plots for the nine modifier loci that modify AO of MJD. Purple line indicates the genetic recombination rate (cM/Mb). SNPs in linkage disequilibrium with identified are shown in color gradient indicating r2 levels (hg19, 1KGP, Nov 2014, EUR).

Supplementary Tables

Supplementary Table 1. Linear relationship between AO and CAG_{exp}, CAG_{nor}, geographical origin, sex and pairwise interaction of the given factors. A total of 62.7 % of the variability in the AO is explained by given factors.

Model description	Multiple R^2	Adjusted R^2	P-value	ΔR^2
AO ~ CAG_{exp}	0.6200	0.6195	$<2.2 \times 10^{-16}$	
AO ~ CAG_{exp} + origin	0.6241	0.6216	$<2.2 \times 10^{-16}$	0.0021
AO ~ CAG_{exp} + origin + sex	0.6265	0.6235	$<2.2 \times 10^{-16}$	0.0019
AO ~ CAG_{exp} + origin + sex + CAG_{nor}	0.6282	0.6247	$<2.2 \times 10^{-16}$	0.0012
AO ~ CAG_{exp} + origin + sex + CAG_{nor} + CAG_{exp}:CAG_{nor}	0.6301	0.6261	$<2.2 \times 10^{-16}$	0.0014
AO ~ CAG_{exp} + origin + sex + CAG_{nor} + CAG_{exp}:CAG_{nor} + CAG_{exp}:origin	0.6328	0.6267	$<2.2 \times 10^{-16}$	0.0006
AO ~ CAG_{exp} + origin + sex + CAG_{nor} + CAG_{exp}:CAG_{nor} + CAG_{exp}:origin + CAG_{nor}:origin	0.6352	0.6271	$<2.2 \times 10^{-16}$	0.0004

Supplementary Table 2. Subjects and cohort demographics.

Geographical origin	# of patients	Mean (SD) AO	M:F
Portugal	330	40.0 (±12.4)	1.0
Brazil	311	34.9 (±11.7)	1.1
North America	55	37.8 (±12.2)	0.7
Germany	51	37.6 (±9.2)	1.2
NA	34	37.1 (±11.1)	1.4
Australia	5	52.8 (±10.1)	0.3

M:F - male-female ratio.

Please browse Full Text version to see the data of Supplementary Tables 3 and 4.

Supplementary Table 3. Functional annotation of SNPs. rsID: reference SNP ID; MAF: minor alelle frequency; r^2: the maximum r^2 of the SNP with one of the independent significant SNPs; nearest gene: the nearest Gene of the SNP based on ANNOVAR annotations; distance: distance to the nearest gene; func: functional consequence of the SNP on the gene obtained from ANNOVAR; CADD: CADD score which is computed based on 63 annotations.

Supplementary Table 4. Previously identified HD-AO modifier loci in MJD.

Supplementary Table 5. Gene sets and pathways enriched in i-GSEA4GWAS.

Pathway/Gene set name	Gene Set ID	P-value	FDR
GO: TRANSPORT VESICLE	GO:0030133	0.001	0.0082
KEGG: OLFACTORY TRANSDUCTION	hsa04740	0.001	0.0083
Olfactory Signaling Pathway	R-HSA-381753	0.001	0.0088
GO: SYNAPSE PART	GO:0044456	0.001	0.0093
Synthesis of bile acids and bile salts via 24-hydroxycholesterol	R-HSA-193775	0.001	0.0095
Negative feedback regulation of MAPK pathway	R-HSA-5674499	0.001	0.0101
Purine salvage	R-HSA-74217	0.001	0.0106
GO: METALLOEXOPEPTIDASE ACTIVITY	GO:0008235	0.001	0.0109
GO: SYNAPSE	GO:0045202	0.001	0.0115
GO: MONOCARBOXYLIC ACID TRANSPORT	GO:0015718	0.001	0.0133
GO: OUTER MEMBRANE	GO:0019867	0.001	0.0141
GO: AMINOPEPTIDASE ACTIVITY	GO:0004177	0.001	0.015
Localization of the PINCH-ILK-PARVIN complex to focal adhesions	R-HSA-446343	0.001	0.0159
BioCarta: PLATELETAPP PATHWAY	M6487	0.001	0.0161
GO: EXOPEPTIDASE ACTIVITY	GO:0008238	0.001	0.018
TFAP2 (AP-2) family regulates transcription of other transcription factors	R-HSA-8866906	0.001	0.0212
GO: MITOCHONDRIAL OUTER MEMBRANE	GO:0005741	0.001	0.0215
GO: ORGANELLE OUTER MEMBRANE	GO:0031968	0.003	0.0216
GO: HISTONE DEACETYLASE COMPLEX	GO:0000118	0.001	0.0218
Fanconi Anemia Pathway	R-HSA-6783310	0.001	0.0221
GO: PROTEASOME COMPLEX	GO:0000502	0.001	0.0221
GO: RECEPTOR MEDIATED ENDOCYTOSIS	GO:0006898	0.001	0.0225
GO: GABA RECEPTOR ACTIVITY	GO:0016917	0.001	0.0226
Metabolism of Angiotensinogen to Angiotensins	R-HSA-2022377	0.001	0.0231
GO: TRANS GOLGI NETWORK TRANSPORT VESICLE	GO:0030140	0.001	0.0236
Calcitonin-like ligand receptors	R-HSA-419812	0.001	0.0242
GO: MONOCARBOXYLIC ACID TRANSMEMBRANE TRANSPORTER ACTIVITY	GO:0008028.	0.001	0.0245
HDL remodeling	R-HSA-8964058	0.001	0.0262
Synthesis of epoxy (EET) and dihydroxyeicosatrienoic acids (DHET)	R-HSA-2142670	0.001	0.0263
GO: RESPONSE TO HORMONE STIMULUS	GO:0009725	0.001	0.0273
GO: PEPTIDE METABOLIC PROCESS	GO:0006518	0.004	0.0348
GRB7 events in ERBB2 signaling	R-HSA-1306955	0.001	0.0348
Mitochondrial Uncoupling Proteins	R-HSA-166187	0.008	0.0354
The fatty acid cycling model	R-HSA-167826	0.008	0.0354
The proton buffering model	R-HSA-167827	0.008	0.0354
ATF6 (ATF6-alpha) activates chaperone genes	R-HSA-381183	0.002	0.037
GO: GOLGI ASSOCIATED VESICLE	GO:0005798	0.003	0.0371
Free fatty acids regulate insulin secretion	R-HSA-400451	0.001	0.0374
GO: XENOBIOTIC METABOLIC PROCESS	GO:0006805	0.001	0.0382
GO: DENDRITE	GO:0030425	0.001	0.0386
Beta-oxidation of pristanoyl-CoA	R-HSA-389887	0.001	0.0413
Toxicity of botulinum toxin type D (BoNT/D)	R-HSA-5250955	0.001	0.0414

Toxicity of botulinum toxin type F (BoNT/F)	R-HSA-5250981	0.001	0.0414
Processing and activation of SUMO	R-HSA-3215018	0.001	0.0416
KEGG: NUCLEOTIDE EXCISION REPAIR	hsa03420	0.001	0.0422
GO: RESPONSE TO XENOBIOTIC STIMULUS	GO:0009410	0.001	0.0462

Please browse Full Text version to see the data of Supplementary Tables 6, 7.

Supplementary Table 6. Gene sets and pathways enriched in i-GSEA4GWAS.

Supplementary Table 7. Top gene sets and pathways enriched in PASCAL.